Structural analysis of $LaVO_3$ thin films under epitaxial strain

H. Meley, Karandeep, L. Oberson, J. de Bruijckere, D. T. L. Alexander, J.-M. Triscone, Ph. Ghosez, and S. Gariglio

Citation: APL Materials **6**, 046102 (2018); doi: 10.1063/1.5021844
View online: https://doi.org/10.1063/1.5021844
View Table of Contents: http://aip.scitation.org/toc/apm/6/4
Published by the American Institute of Physics

Structural analysis of $LaVO_3$ thin films under epitaxial strain

H. Meley,[1,a] Karandeep,[2] L. Oberson,[3] J. de Bruijckere,[1,b]
D. T. L. Alexander,[3] J.-M. Triscone,[1] Ph. Ghosez,[2] and S. Gariglio[1]
[1]*DQMP, University of Geneva, 24 Quai E.-Ansermet, CH-1211 Geneva, Switzerland*
[2]*Physique Théorique des Matériaux, Université de Liège (B5), B-4000 Liège, Belgium*
[3]*Interdisciplinary Centre for Electron Microscopy (CIME), École Polytechnique Fédérale de Lausanne (EPFL), CH-1015 Lausanne, Switzerland*

(Received 9 January 2018; accepted 12 March 2018; published online 4 April 2018;
corrected 6 April 2018)

Rare earth vanadate perovskites exhibit a phase diagram in which two different types of structural distortions coexist: the strongest, the rotation of the oxygen octahedra, comes from the small tolerance factor of the perovskite cell ($t = 0.88$ for $LaVO_3$) and the smaller one comes from inter-site d-orbital interactions manifesting as a cooperative Jahn-Teller effect. Epitaxial strain acts on octahedral rotations and crystal field symmetry to alter this complex lattice-orbit coupling. In this study, $LaVO_3$ thin film structures have been investigated by X-ray diffraction and scanning transmission electron microscopy. The analysis shows two different orientations of octahedral tilt patterns, as well as two distinct temperature behaviors, for compressive and tensile film strain states. *Ab initio* calculations capture the strain effect on the tilt pattern orientation in agreement with experimental data. https://doi.org/10.1063/1.5021844

Complex oxides with perovskite structures display a variety of physical properties, some being insulators, others superconductors, some showing ferroelectricity, and others ferromagnetic or charge orders.[1] With chemical formula ABO_3, the oxide perovskite unit cell adapts to the A and B cations by changing its crystal symmetry according to the tolerance factor t, defined as the ratio between the cation-oxygen distances ($t = [R_A + R_O]/[\sqrt{2}(R_B + R_O)]$ with R_A, R_O, and R_B being the A, O, and B ionic radii). t signals if the AO or the BO bonds are under tension or compression: for t equal to one, one observes a cubic symmetry. For t larger than one, the system is prone to a ferroelectric-type structural instability with a displacement of the B cation in the AO cage. For t smaller than one, the oxygen octahedron rotates with a specific pattern, allowing the A cations to come closer.[2] 15 tilt patterns of the oxygen octahedron have been identified and observed experimentally.[3,4]

Among them, the most common occurs in the orthorhombic *Pbnm* structure,[5,6] where the octahedra rotate out-of-phase along 2 axes of the pseudo-cubic perovskite structure (or in-phase along the plane diagonal) and in-phase along the other one, described as an ($a^-a^-c^+$) tilt pattern according to the Glazer notation.[7] Consequently, an anti-polar motion consisting in opposite motions of the A cations in consecutive (0 0 1) planes appears. An illustration of these structural distortions is shown in Fig. 1. In this particular tilt pattern, the O cages' rotation (Φ^-_{xy}, Φ^+_z) and the motion of A cations' plane (X^-_5) are coupled in the Ginzburg-Landau free energy via a trilinear term $\Phi^-_{xy}\Phi^+_z X^-_5$.[6,8] Based on this observation, a set of theoretical proposals has recently been advanced to create an artificial ferroelectric material by stacking ABO_3/A'BO_3 orthorhombic layers and hence breaking the dipole compensation.[9–11] For these heterostructures, the X^-_5 mode is not the primary order parameter but is imposed by octahedral rotations; therefore, hybrid improper ferroelectricity is expected.[12–14] Since the vanadate perovskites display the required orthorhombic symmetry, they stand as good candidates

[a]hugo.meley@unige.ch
[b]Now at Delft University of Technology, Lorentzweg 1, 2628 CJ Delft, The Netherlands.

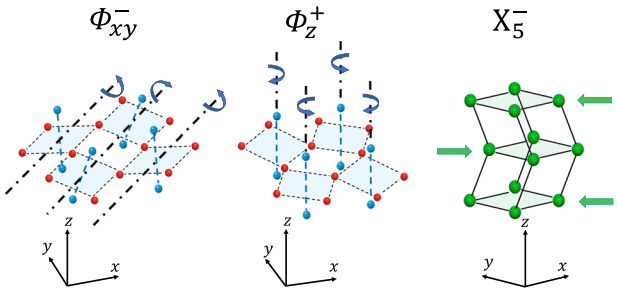

FIG. 1. Illustration of distortion modes in orthorhombic peroskite structures. Red and blue spheres represent the planar and apical oxygen atoms, while the green spheres represent the A cations. The in-plane ϕ_{xy}^{-} rotations are out of phase ($^-$) with respect to the pseudo-cubic reference system (in-phase along the plane diagonal), while the ϕ_z^+ rotations about the vertical z axis are in phase ($^+$). The X_5^- mode generates dipoles, indicated by the arrows, stacked in an antiferroelectric arrangement.

for such a ferroic state. Moreover, they harbour an antiferromagnetic order, coupled to an orbital order, which potentially could also be modified by polarization switching.[8] Nevertheless, the achievement of hybrid improper ferroelectricity in such heterostructures remains an open question since growth on a crystalline substrate can inhibit octahedral rotations. For instance, recent work revealed that octahedral rotations can be suppressed in $SrRuO_3$ layers when stacked with undistorted perovskite cells like $SrTiO_3$ or $BaTiO_3$, leading to modified electronic properties.[15]

Here, we investigate epitaxial constraint effects in a series of $LaVO_3$ thin films grown on different substrates providing compressive and tensile biaxial strain. High-resolution X-ray diffraction (XRD) and scanning transmission electron microscopy (STEM) reveal that the films minimize strain by assuming different tilt pattern orientations, i.e., different anti-polar mode orientations in space. In the second part, using temperature dependent XRD, we show that strain also alters the natural bulk structural transition. For the compressive case, we observe that the structural transition, occurring in bulk from orthorhombic to monoclinic at 140 K upon cooling, is suppressed.

At room temperature, $LaVO_3$, the V^{3+} perovskite family member with the largest rare earth cation, has an orthorhombic structure (*Pbnm*, $a = 5.555$ Å, $b = 5.553$ Å, $c = 7.8486$ Å), with octahedral rotation angles of 12° and 8°, respectively, around the z and xy directions, z being parallel to the orthorhombic long axis.[16] The distorted lattice splits the crystal field of the V t_{2g} orbitals by some meV and favours a M-type Jahn-Teller distortion of the octahedra.[8] However, neutron diffraction indicates that the three V–O bond lengths are quasi-equal;[17] this observation has been attributed to quantum orbital fluctuations within the t_{2g} states, which lead to a quasi-even occupation of the d_{xy}, d_{xz}, and d_{yz} orbitals.[18,19] At ∼140 K, a phase transition from an orbital fluctuation regime to a G-type orbitally ordered state occurs, see Fig. 2. Interestingly, this ground state is not induced by the tilt pattern which, via an M-type JT distortion, would have favoured a C-type orbital ordering (O.O) but results from inter-site d orbital correlations along the z axis. In the present case, G-Type O.O. drives $LaVO_3$ into a monoclinic phase ($P2_1/m$),[20] where planar O–V–O bond lengths become shortened/lengthened by 3%-4% in a checkerboard fashion due to electron occupancy of d_{xy}/d_{yz} and d_{xy}/d_{xz} in two consecutive V sites; the O.O. also leads to a shortening of the c_o axis. Concomitantly, a C-type spin ordering establishes.[18,19,21,22] Above and below the transition, the system remains insulating since a large on-site Coulomb repulsion determines a sizable Mott gap of 1 eV.[23,24]

Recently, density functional theory (DFT) and dynamical mean-field theory (DMFT) calculations have investigated epitaxial strain effects on the electronic structure of $LaVO_3$ thin films.[22,25] Theory predicts that a biaxial strain applied to the (0 0 1) pseudo-cubic plane does not substantially modify the band gap but can alter the ground state spin and orbital orders.

For this study, $LaVO_3$ thin films are grown on cubic (0 0 1)-oriented $SrTiO_3$ substrates to induce a compressive strain of ∼−0.5% and on $(110)_o$-oriented $DyScO_3$ substrates to induce a tensile strain of ∼+0.5%.[26] The $LaVO_3$ layers are grown by pulsed laser deposition (PLD) using an excimer KrF laser run at 1 Hz repetition rate and at high pulse fluence (2 J/cm^2). Deposition occurs on substrates heated from 800 °C to 900 °C in a 5×10^{-7} mbar oxygen atmosphere from a ceramic target of $LaVO_4$; cooling is performed in the same oxygen pressure.[27] *In situ* reflection high energy electron diffraction

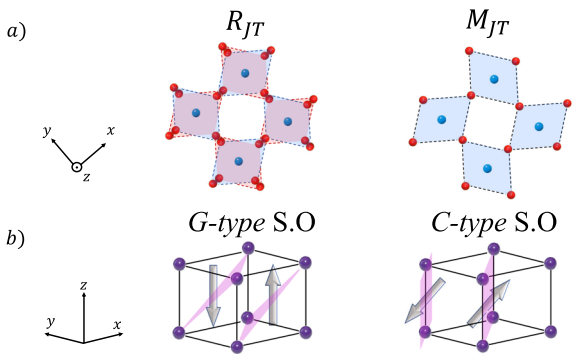

FIG. 2. Illustration of Jahn-Teller-type collective distortions and spin orders. (a) The *R*-type JT distortion exchanges the directions of contraction/elongation of the V–O bond length along the vertical *c* axis while, in the *M*-type JT distortion, these directions remain fixed. Orbital orders and JT distortions are then coupled: C-type O.O. for the R_{JT} distortion and G-type O.O. for the M_{JT} one. (b) The spin orders are determined by the orbital orders. For the R_{JT} distortion and the C-type O.O., the spins align ferromagnetically on (1 1 1) planes (in violet) and anti-ferromagnetically between the planes (G-type S.O.); in the case of the M_{JT} distortion and G-type O.O., the spins are coupled ferromagnetically on (1 1 0) planes and anti-ferromagnetically between the planes (C-type S.O.).

(RHEED) reveals that the deposition evolves from a layer-by-layer growth mode during the first few unit cells (u.c.) to a mainly step-flow mode. Atomic force microscopy (AFM) exposes the high surface quality of the layers: 80 nm thick film topography shown in Fig. 3 displays a step-and-terrace structure, mirroring the $(110)_o$ $DyScO_3$ substrate surface.

Samples for STEM were prepared by a combination of mechanical polishing using an Allied High Tech MultiTech polishing system, followed by argon ion beam milling with a Gatan PIPS II system to electron transparency. High angle annular dark field (HAADF) STEM images of these samples were acquired using a double aberration-corrected FEI Titan Themis 60-300 operated at a high tension of 300 kV. In addition, annular bright field (ABF) images were acquired on the sample of $LaVO_3$ on $DyScO_3$ in order to visualize the O sites. In order to reduce artefacts from system noise and scan drift, each presented image is the average of a series of rapidly acquired images that underwent rigid and non-rigid alignment using the Smart Align software.[28] The cation column positions were then identified with a few pm precision using the Ranger code.[29] From these, in order to highlight the A site charge ordering, effective atomic strain maps for these sites were determined by their strain displacements relative to the mean unit cell position for each site.

Figure 3 shows crystal truncation rods measured by XRD close to the $(002)_{pc}$ substrate reflection: finite-size fringes due to the high crystalline coherence along the growth direction are observed around the film reflection.[30] A fit of these oscillations yields an estimation of the layer thickness of 80 nm. A reciprocal space map of the $(103)_{pc}$ reflections for $SrTiO_3$ substrate and $LaVO_3$ film shows a matching of in-plane lattice parameters, see the inset of Fig. 3, indicating a coherent strained state. Rocking curves around the layer reflections do not reveal the presence of dislocations.[31]

Biaxial strain applied on a $\{100\}_{pc}$ oriented perovskite induces a tetragonal distortion that anisotropically modifies the AO and BO bonds' length and, as a consequence, the octahedral rotations and/or tilt pattern for compounds with $t < 1$. In most cases, a change of rotation angles is observed and, more rarely, a new tilt pattern emerges, as recently observed in strained rhombohedral films.[32,33] In order to determine the tilt pattern of a strained layer, the common experimental approach consists in probing with X-rays different families of half-integer Bragg reflections. Within the pseudo-cubic basis, half-order Bragg peaks exist because of octahedral rotations and A cation displacement that lower the original cubic symmetry into an irreducible unit cell representation, orthorhombic for $LaVO_3$.[34] Measuring precisely the intensity of these half-order peaks allows the refinement of the crystal structure and its distortions.[35] This often requires synchrotron radiation to quantify the rotation angles and the lanthanum displacements. Here, we take advantage of the strong intensity of the half integer peaks produced by the X_5^- mode, only present in the $a^-b^-c^+$ phase, to determine the tilt system using a laboratory diffraction setup.

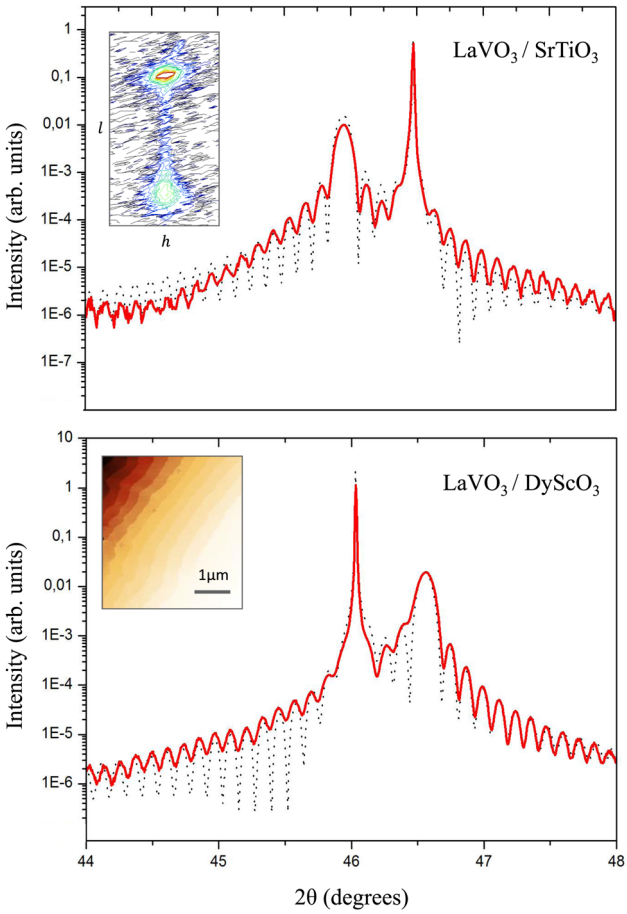

FIG. 3. Characterization of $LaVO_3$ films. $\theta - 2\theta$ scans around the $(002)_{pc}$ reflection of $LaVO_3$ layers show finite size effects: the fits yield a layer thickness of 80 nm for both films. Upper inset: reciprocal space map around $(103)_{pc}$ $LaVO_3$ and $DyScO_3$ peaks, revealing that the film remains coherently strained to the substrate. Lower inset: a 4 μm × 4 μm AFM image of the film surface shows unit cell steps and terraces.

In this paper, we express the layer Bragg reflections in the pseudo-cubic basis, with the l index parallel to the out of plane direction. In order to determine the layers' tilt pattern orientation, $\{0\ \frac{1}{2}\ 1\}_{pc}$ half-integer Bragg reflections were probed. In $a^-b^-c^+$ tilt systems, the A cations, coupled to octahedra antiferrodistortive (AFD) motions, move within the xy plane in the opposite direction between two consecutive $(001)_{pc}$ planes; this is the previously mentioned antipolar X_5^- mode that produces an extra diffraction peak $\{0\ \frac{1}{2}\ 1\}_{pc}$. The associated diffracted intensity is non-zero if the half-integer index matches the antipolar mode plane index. Furthermore, A cations move in the xy plane along the $\alpha\hat{x} + \beta\hat{y}$ vector, the α/β ratio being proportional to the $(1\ 0\ \frac{1}{2})_{pc}/(0\ 1\ \frac{1}{2})_{pc}$ reflections' intensity ratio. Since the orthorhombic unit cell is defined with a and b lattice parameters in the antipolar mode plane, the identification of $\{0\ \frac{1}{2}\ 1\}_{pc}$ peaks determines the tilt pattern orientation.

Figure 4 [panels (a), (c), and (d)] shows reciprocal space maps for a film deposited on a cubic $SrTiO_3$ substrate: only the $(0\ \frac{1}{2}\ 1)_{pc}$ and $(\frac{1}{2}\ 0\ 1)_{pc}$ peaks are observed, while the $(0\ 1\ \frac{1}{2})_{pc}$ and $(1\ 0\ \frac{1}{2})_{pc}$ reflections are absent. The observed reflections indicate that the film presents the long orthorhombic c-axis (c_o) aligned parallel to the substrate surface. This is indeed the orientation that minimizes the film stress and, since the surface of $SrTiO_3$ has a square symmetry, we observe domains with c_o parallel to the two in-plane axes of $SrTiO_3$, in agreement with previous findings.[34,36] For the tensile strain, mismatch minimization suggests that c_o should be directed out-of-plane. This is confirmed by the XRD data of a $LaVO_3$ film deposited on a $(110)_o$ $DyScO_3$ crystal. Figure 4 [panels (b), (e), and (f)] displays the $(0\ 1\ \frac{1}{2})_{pc}$ and $(1\ 0\ \frac{1}{2})_{pc}$ reflections' intensities, which are only compatible with the

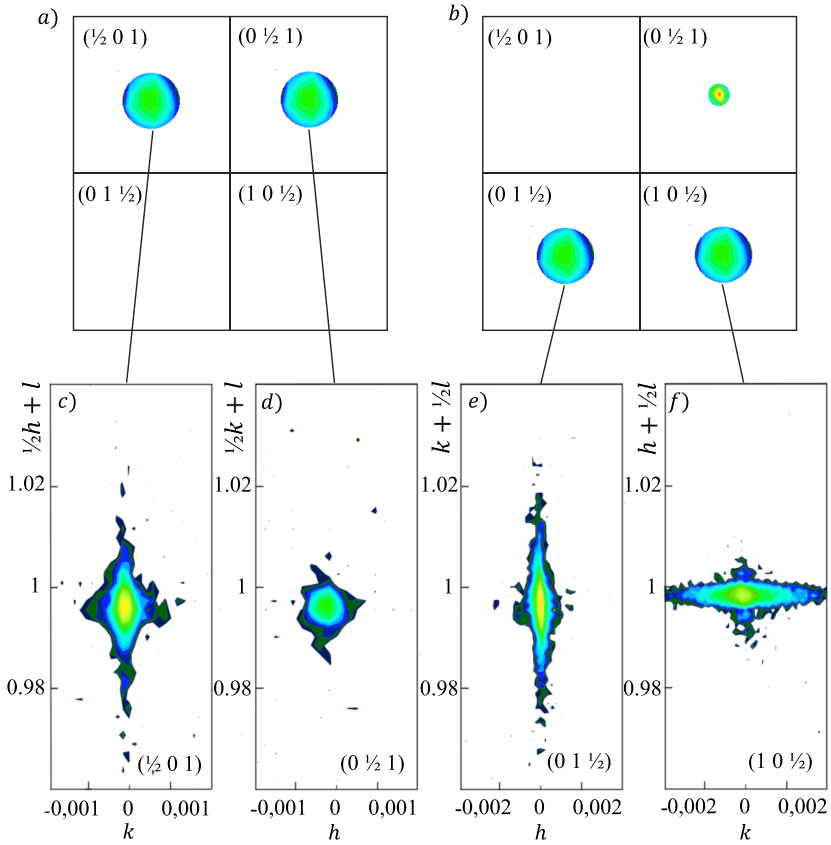

FIG. 4. Half-order reflections for the $\{0\ \frac{1}{2}\ 1\}_{pc}$ plane family revealing the tilt pattern of the layers. [(a), (c), and (d)] For a $LaVO_3$ film deposited on a cubic $SrTiO_3$ substrate, Q-maps show intensity for $(\frac{1}{2}\ 0\ 1)_{pc}$ and $(0\ \frac{1}{2}\ 1)_{pc}$ reflections while $(1\ 0\ \frac{1}{2})_{pc}$ and $(0\ 1\ \frac{1}{2})_{pc}$ are absent. [(b), (e), and (f)] A $LaVO_3$ layer grown onto $(110)_o$ oriented $DyScO_3$ displays a peak only for the $(0\ 1\ \frac{1}{2})_{pc}$ and $(1\ 0\ \frac{1}{2})_{pc}$ reflections; $(\frac{1}{2}\ 0\ 1)_{pc}$ and $(0\ \frac{1}{2}\ 1)_{pc}$ are absent. The intensity for the $(0\ \frac{1}{2}\ 1)_{pc}$ reflection originates from the substrate.

$a^-b^-c^+$ tilt pattern. Table I provides the orthorhombic lattice parameters and tilt patterns for layers and substrates extracted from XRD data analysis.

To image the distorted lattice structures of the layers in real-space, atomic resolution HAADF-STEM-imaging has been performed to measure the A site and B site cation positions across the substrate/layer interfaces and within the layers. In the current work, we focus on the distortions inside the layers and we do not investigate the transition zone between the rotation pattern of the

TABLE I. Summary of the XRD data acquired at room temperature for $LaVO_3$ films grown on different substrates. The layer parameters are calculated for an orthorhombic structure.

Substrate					
	Tilt pattern	a_o (Å)	b_o (Å)	c_o (Å)	γ (deg)
$SrTiO_3$	$a^0a^0a^0$	Cubic 3.905 (Å)			
$DyScO_3$	$a^-a^-c^+$	5.714	5.438	7.897	90
$LaVO_3$ layer					
Grown on	Tilt pattern	a_o (Å)	b_o (Å)	c_o (Å)	γ (deg)
(001) $SrTiO_3$	$a^-b^+c^-$	5.554	5.551	7.8111	89.39
$(110)_o$ $DyScO_3$	$a^-b^-c^+$	5.580	5.580	7.7948	90.08

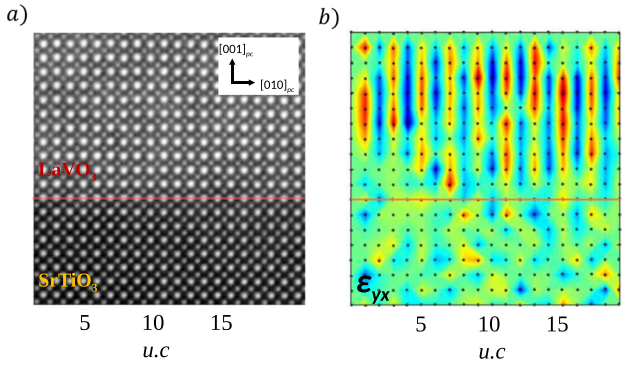

FIG. 5. (a) HAADF STEM image of a 20 × 20 (pseudocubic) u.c. area of $LaVO_3/SrTiO_3$ interface; brightest spots corresponding to the La and Sr atom columns and darker spots to the V and Ti columns. The interface is imaged along the $SrTiO_3$ [100] zone axis. We can clearly see by contrast the sharp interface between the layer and substrate. (b) Strain mapping of La and Sr cation displacement. The strain tensor matrix element ϵ_{yx} shows that the layer X_5^- mode starts sharply at the interface.

substrate and one of the films. In our view, this is motivated by the short distance [few unit cells (u.c.)] over which such transition occurs[37,38] that should not affect the physics occurring in 200 u.c. thick films. This approach is also in line with the DFT calculations where only the in-plane epitaxial strain effect is taken into account and not the octahedral configuration of the underlying substrate.

Within the scanned areas, the imaging revealed the high quality of the films, identifying no defects and perfect epitaxy in the samples of $LaVO_3$ on $SrTiO_3$ or $DyScO_3$, as shown, respectively, in Figs. 5 and 6.[39] Strain mapping of the La columns clearly shows the X^{5-} mode, as demonstrated in the right panels of Figs. 5 and 6. Figure 6 also demonstrates the O octahedral rotations in the $LaVO_3$ on $DyScO_3$ via ABF imaging. The displacements reveal the two different orientations of the orthorhombic long c axis that lies in-plane for compressive ($LaVO_3/SrTiO_3$) and out-of-plane for tensile strain ($LaVO_3/DyScO_3$), in agreement with the XRD analysis.

The ground-state configuration of the $LaVO_3$ layer under biaxial epitaxial strains has been calculated from first-principles using density functional theory (DFT) and projector augmented-wave (PAW) approach as implemented in the Vienna *ab initio* simulation package (VASP).[40] We used the Perdew-Burke-Ernzerhof revised for solids (PBEsol) exchange-correlation functional. To include the

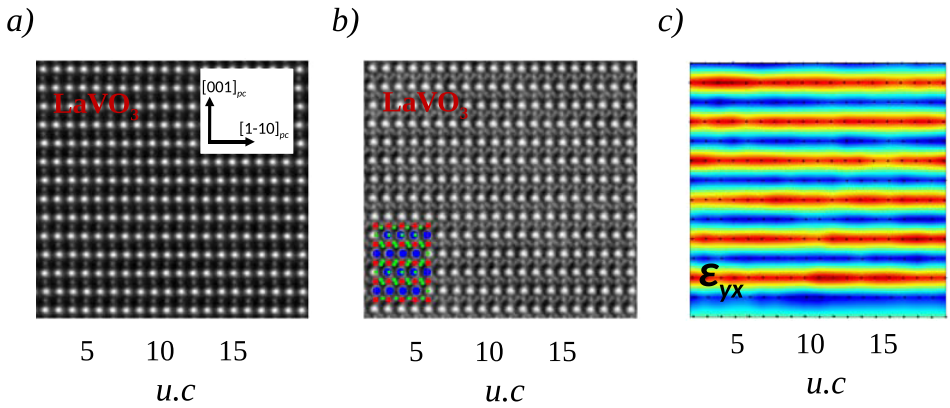

FIG. 6. (a) HAADF STEM image of a 19 × 13 (pseudocubic) u.c. area of the $LaVO_3$ layer grown on a $DyScO_3$ substrate; brightest spots corresponding to the La columns and darker spots to the V ones. The sample is imaged along the $DyScO_3$ $[001]_o$ zone axis. (b) Simultaneously acquired ABF image with inverted contrast allows the O columns to be visualized, demonstrating the O octahedral rotations from their canted positions in the projection. To show structural correspondence, the DFT calculated model is overlaid on the image (La in blue, V in red, and O in green). (c) Strain mapping of La cation displacement in the HAADF image: the strain tensor matrix element ϵ_{yx} shows the X_5^- mode where $(001)_o$ La planes move corresponding to a $a^-b^-c^+$ tilt pattern.

effect of strong correlations among vanadium d-electrons, an on-site Coulomb repulsion $U = 3.5$ eV has been included.[8] Calculations have been performed on a $2 \times 2 \times 2$ (40-atom) supercell. The effect of the epitaxial strain has been imposed by constraining the in-plane lattice constants of the supercell to a square lattice with the lattice parameter equivalent to that of $SrTiO_3$ or of pseudo-cubic $DyScO_3$. All structures have been relaxed until the forces on the atoms are less than 10^{-4} eV/Å with an energy convergence of 10^{-9} eV. Convergence is achieved by using a planewave cutoff of 500 eV and $4 \times 4 \times 4$ k-point mesh. For distinct in-plane strains, calculations have been performed for different orbital and spin orderings and different crystal orientations.

For the symmetry of the layer, we note that epitaxy from a square lattice substrate constrains the layer in-plane lattice axes and angles but leaves the out-of-plane pseudo-cubic c_{pc} axis free to adapt. As a consequence, for a growth with c_o perpendicular to the substrate plane, a_o and b_o are equal and the angle γ between them is 90°: the film can maintain the *Pbnm* and $P2_1/m$ symmetries of the bulk. In the case of a growth with c_o in the substrate plane, a change in c_{pc} results in a modification of a_o and b_o and, as soon as $\gamma \neq 90°$, it induces lowering of symmetry from *Pbnm* to $P2_1/m$ and from $P2_1/m$ to $P2_1$. In the case $a_o \neq b_o$, the $[110]_o$ layer direction is canted from the normal to the substrate plane. Since such a canting can in practice be prevented when different domains coexist,[41] calculations have also been performed forcing the film to remain straight.

Figure 7 shows the result of the calculations for different strain states: we see that the theory correctly predicts the experimentally observed configuration. For the growth on $SrTiO_3$, the growth orientation with c_o in-plane (canted and non-canted films) is preferred over that with c_o out-of-plane: although theoretically the ground-state structure is canted, experimentally we do not observe such canting, in line with the detection of structural domains with c_0 at 90° as highlighted earlier, and the film remains straight. When a tensile strain is applied to the layer by the $DyScO_3$ substrate, the lowest energy configuration is this time with c_o oriented out-of-plane. Since $DyScO_3$ is not cubic, additional calculations have been performed taking into account the orthorhombicity of the substrate but without changing the result.

On the two substrates, the type of orbital order affects less energy than the crystal orientation. Still, on $SrTiO_3$ with c_o in-plane growth in the not-canted structure, the ground-state O.O. is predicted to be of C-type; on $DyScO_3$ with c_o out-of-plane growth, the two orbital orders are nearly degenerated but with the tendency to stabilise a more G-type O.O. ground state under such tensile strain.

As previously discussed, the orbital and magnetic orders in $LaVO_3$ bulk establish below 140 K, where a phase transition occurs between an orbital fluctuation regime with M-type JT-distortions to

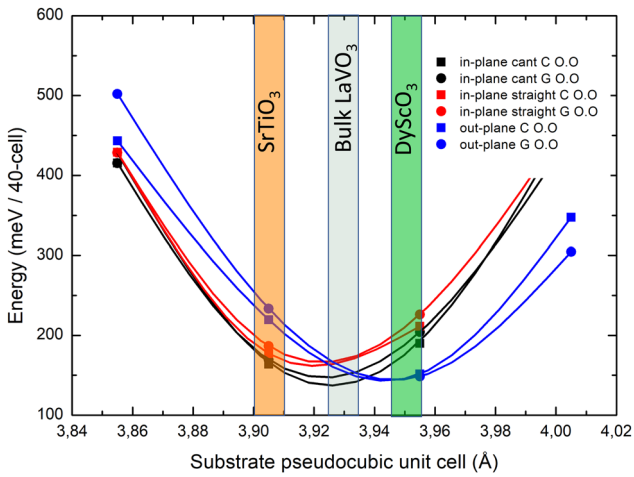

FIG. 7. Energy-strain phase diagram of epitaxial $LaVO_3$ thin films. The energy of several structures is calculated imposing a strain from a cubic substrate and assuming different orbital orders (respectively, G-type or C-type) and corresponding magnetic order (respectively, C-type or G-type). In-plane and out-plane notations refer to the orientation of the layer c_o axis with respect to the plane of the substrate while G O.O. and C O.O. are the two types of orbital orders. For c_o in-plane, both the cases of straight and canted films have been considered.

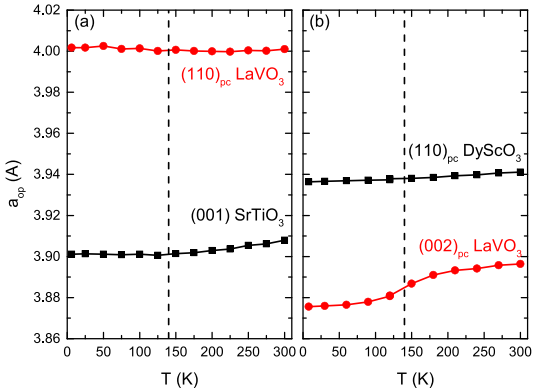

FIG. 8. Temperature evolution of the pseudo-cubic out-of-plane lattice parameter (a_{op}) for (a) compressive strain ($LaVO_3/SrTiO_3$) and (b) tensile strain ($LaVO_3/DyScO_3$). The vertical lines indicate the temperature for the Jahn-Teller-induced structural transition in bulk.

a G-type orbitally ordered state with *R*-type JT-distortions. This electronic phase transition is also manifested as a structural change, with a contraction of c_o and expansion of a_o and b_o.[42]

With the purpose to reveal a possible structural phase transition in the films, the evolution in temperature of the out-of-plane lattice parameter (a_{op}) has been followed by XRD for the layers in compressive and tensile strain.[43] The left panel of Fig. 8 shows the compressively strained $LaVO_3$ layer: we do not observe any change of the out-of-plane lattice parameter. On the other hand, the $LaVO_3$ layer grown on $DyScO_3$ under tensile strain shows a clear, smooth transition (see the right panel of Fig. 8). For this orientation, the system can lower its symmetry and shrink the c_o axis to accommodate the G-type O.O.: this reduction of a_{op} is known to be associated with the transition from an *M*-type JT-distortion to an *R*-type JT-distortion. For the layers on $SrTiO_3$, the c_o axis is locked by epitaxy to the substrate: we would consequently expect that the system condenses in a C-type O.O. in agreement with the theoretical prediction, developing the *M*-type JT-distortions already present in the room temperature monoclinic structure. Ongoing investigation into the orbital and spin order will shed light on the exact electronic ground state of these films.

In summary, a detailed structural study, supported by DFT calculations, shows that the orthorhombic structure accommodates the epitaxial strain by assuming different rotation patterns of the oxygen octahedra. The evolution in temperature of the structure suggests that epitaxy affects the orbital order of the ground state. The relation uncovered here between the strain and growth direction may be relevant for the achievement of improper ferroelectrics by stacking anti-polar modes in artificially symmetry-breaking heterostrucutres.

See supplementary material for details on phase matching between epitaxial layer and substrate, and orthorombic distortion modes analysis.

The authors thank B. Mallett and Ch. Bernard of the University of Fribourg for their help in the low temperature XRD measurements and Daniéle Laub and Colette Vallotton of CIME, EPFL for the STEM sample preparation. This work was supported by the Swiss National Science Foundation - division II, by the Synergia Project No. 154410 and has received funding from the European Research Council under the European Union Seventh Framework Programme (No. FP7/2007-2013)/ERC Grant Agreement No. 319286 (Q-MAC). Ph.G. acknowledges financial support from ARC project AIMED and F.R.S.-FNRS PDR project HiT4FiT. K.D. was supported by the University of Liege and the EU in the context of the FP7-PEOPLE-COFUND-BeIPD project. Calculations have been performed, thanks to the access to the Céci computing facilities funded by F.R.S-FNRS (Grant No. 2.5020.1) and to the Tier-1 supercomputer of the Fédération Wallonie-Bruxelles funded by the Walloon Region (Grant No. 1117545).

[1] D. I. Khomskii, *Transition Metal Compounds* (Cambridge University Press, 2014).
[2] J. B. Goodenough, Rep. Prog. Phys. **67**, 1915 (2004).
[3] P. M. Woodward, Acta Crystallogr., Sect. B: Struct. Sci. **53**, 44 (1997).
[4] C. J. Howard and H. T. Stokes, Acta Crystallogr., Sect. B: Struct. Sci. **54**, 782 (1998).

[5] N. A. Benedek and C. J. Fennie, J. Phys. Chem. **117**, 13339 (2013).
[6] N. Miao, N. C. Bristowe, B. Xu, M. J. Verstraete, and P. Ghosez, J. Phys.: Condens. Matter **26**, 035401 (2014).
[7] A. M. Glazer, Acta Crystallogr., Sect. B: Struct. Crystallogr. Cryst. Chem. **28**, 3384 (1972).
[8] J. Varignon, N. C. Bristowe, E. Bousquet, and P. Ghosez, Sci. Rep. **5**, 15364 (2015).
[9] J. M. Rondinelli and C. J. Fennie, Adv. Mater. **24**, 1961 (2012).
[10] N. A. Benedek, A. T. Mulder, and C. J. Fennie, J. Solid State Chem. **195**, 11 (2012).
[11] N. A. Benedek, J. M. Rondinelli, H. Djani, P. Ghosez, and P. Lightfoot, Dalton Trans. **44**, 10543 (2015).
[12] E. Bousquet, M. Dawber, N. Stucki, C. Lichtensteiger, P. Hermet, S. Gariglio, J.-M. Triscone, and P. Ghosez, Nature **452**, 732 (2008).
[13] N. A. Benedek and C. J. Fennie, Phys. Rev. Lett. **106**, 107204 (2011).
[14] H. J. Zhao, J. Íñiguez, W. Ren, X. M. Chen, and L. Bellaiche, Phys. Rev. B **89**, 174101 (2014).
[15] D. Kan, R. Aso, R. Sato, M. Haruta, H. Kurata, and Y. Shimakawa, Nat. Mater. **15**, 432 (2016).
[16] P. Bordet, C. Chaillout, M. Marezio, Q. Huang, A. Santoro, S.-W. Cheong, H. Takagi, C. Oglesby, and B. Batlogg, J. Solid State Chem. **106**, 253 (1993).
[17] M. J. Martínez-Lope, J. A. Alonso, M. Retuerto, and M. T. Fernéndez-Díaz, Inorg. Chem. **47**, 2634 (2008).
[18] G. Khaliullin, P. Horsch, and A. M. Oleś, Phys. Rev. Lett. **86**, 3879 (2001).
[19] M. De Raychaudhury, E. Pavarini, and O. Andersen, Phys. Rev. Lett. **99**, 126402 (2007).
[20] S. Miyasaka, Y. Okimoto, M. Iwama, and Y. Tokura, Phys. Rev. B **68**, 100406 (2003).
[21] K. I. Kugel' and D. I. Khomskiĭ, Sov. Phys.-Usp. **25**, 231 (1982).
[22] H. Weng and K. Terakura, Phys. Rev. B **82**, 115105 (2010).
[23] T. Arima, Y. Tokura, and J. Torrance, Phys. Rev. B **48**, 17006 (1993).
[24] S. Miyasaka, Y. Okimoto, and Y. Tokura, J. Phys. Soc. Jpn. **71**, 2086 (2002).
[25] G. Sclauzero and C. Ederer, Phys. Rev. B **92**, 235112 (2015).
[26] The subscript *o* indicates planes and orientations in orthorhombic symmetry; the subscript *pc* is used for the pseudo-cubic notation.
[27] Y. Hotta, Y. Mukunoki, T. Susaki, H. Y. Hwang, L. Fitting, and D. A. Muller, Appl. Phys. Lett. **89**, 031918 (2006).
[28] L. Jones, H. Yang, T. J. Pennycook, M. S. J. Marshall, S. Van Aert, N. D. Browning, M. R. Castell, and P. D. Nellist, Adv. Struct. Chem. Imaging **1**, 8 (2015).
[29] L. Jones, http://lewysjones.com/software/ranger/.
[30] The scans were acquired with a X' Pert PRO PanAlytical diffractometer equipped with a Ge(220) monochromator and a triple-axis detector.
[31] S. Gariglio, N. Stucki, J.-M. Triscone, and G. Triscone, Appl. Phys. Lett. **90**, 202905 (2007).
[32] S. J. May, J.-W. Kim, J. M. Rondinelli, E. Karapetrova, N. A. Spaldin, A. Bhattacharya, and P. J. Ryan, Phys. Rev. B **82**, 014110 (2010).
[33] R. L. Johnson-Wilke, D. Marincel, S. Zhu, M. P. Warusawithana, A. Hatt, J. Sayre, K. T. Delaney, R. Engel-Herbert, C. M. Schlepütz, J.-W. Kim, V. Gopalan, N. A. Spaldin, D. G. Schlom, P. J. Ryan, and S. Trolier-McKinstry, Phys. Rev. B **88**, 174101 (2013).
[34] H. Rotella, U. Lüders, P.-E. Janolin, V. H. Dao, D. Chateigner, R. Feyerherm, E. Dudzik, and W. Prellier, Phys. Rev. B **85**, 184101 (2012).
[35] M. Brahlek, A. K. Choquette, C. R. Smith, R. Engel-Herbert, and S. J. May, J. Appl. Phys. **121**, 045303 (2017).
[36] H. Rotella, O. Copie, G. Steciuk, H. Ouerdane, P. Boullay, P. Roussel, M. Morales, A. David, A. Pautrat, B. Mercey, L. Lutterotti, D. Chateigner, and W. Prellier, J. Phys.: Condens. Matter **27**, 175001 (2015).
[37] R. Aso, D. Kan, Y. Shimakawa, and H. Kurata, Sci. Rep. **3**, 2214 (2013).
[38] R. Aso, D. Kan, Y. Shimakawa, and H. Kurata, Cryst. Growth Des. **14**, 2128 (2014).
[39] We note that a different sample of $LaVO_3$ on $DyScO_3$ showed sporadic dislocation loops at an angle to the growth axis within the film bulk but sill maintained perfect epitaxy at the film/substrate interface.
[40] G. Kresse and J. Furthmüller, Phys. Rev. B **54**, 11169 (1996).
[41] O. Copie, J. Varignon, H. Rotella, G. Steciuk, P. Boullay, A. Pautrat, A. David, B. Mercey, P. Ghosez, and W. Prellier, Adv. Mater. **29**, 1604112 (2017).
[42] Y. Ren, A. A. Nugroho, A. A. Menovsky, J. Strempfer, U. Rütt, F. Iga, T. Takabatake, and C. W. Kimball, Phys. Rev. B **67**, 014107 (2003).
[43] We assume that the films remain coherently strained to the substrates during the low temperature cycle.